Article type: Communication

Millivolt Modulation of Plasmonic Metasurface Optical Response via Ionic Conductance

Krishnan Thyagarajan, Ruzan Sokhoyan, Leonardo Zornberg, and Harry A. Atwater[*]

Dr. K. Thyagarajan, Dr. R. Sokhoyan, L. Zornberg, Prof. H. A. Atwater

Thomas J. Watson Laboratory of Applied Physics,

California Institute of Technology,

Pasadena, California 91125, USA

E-mail: haa@caltech.edu

Dr. K. Thyagarajan, Prof. H. A. Atwater

Kavli Nanoscience Institute,

California Institute of Technology,

Pasadena, California 91125, USA

Keywords: Tunable metasurface, filament formation, ionic transport, memristor, indium tin oxide (ITO)

Abstract: We experimentally demonstrate a plasmonic metasurface with an electrically tunable optical response that operates at strikingly low modulation voltages. The fabricated metasurface shows up to 30% relative change in reflectance in the visible spectral range upon application of 5 mV and 78% absolute change in reflectance upon application of 100 mV of bias. The designed metasurface consists of nanostructured silver and indium tin oxide (ITO) electrodes which are separated by 5 nm thick alumina. The millivolt-scale optical modulation is attributed to a new modulation mechanism, in which transport of silver ions through alumina dielectric leads to bias-

Author Manuscript

This is the author manuscript accepted for publication and has undergone full peer review but has not been through the copyediting, typesetting, pagination and proofreading process, which may lead to differences between this version and the Version of Record. Please cite this article as doi: 10.1002/adma.201701044.

This article is protected by copyright. All rights reserved.

induced nucleation and growth of silver nanoparticles in the ITO counter-electrode, altering the optical extinction response. This transport mechanism, which occurs at applied electric fields of 1 mV/nm, provides a new approach to use of ionic transport for electrical control over light-matter interactions.

Article:

Historically, macroscopic optical components, such as lenses, curved mirrors, and polarizers have been used to control the amplitude, polarization, or the phase of light, and modify propagation over distances much larger than the wavelength. Recently, ultrathin nanostructured optical metasurfaces[1, 2] whose thicknesses are comparable to or less than the wavelength have been demonstrated to achieve similar control of light by design of the metasurface phase and amplitude response[2, 3]. For example, metasurface-based holograms[4], ultrathin polarization rotators[5] and flat focusing lens[2] have been previously demonstrated. It has also been proposed that a V-shaped antenna array can be used for on-chip transformation of a single Gaussian beam into four orbital angular momentum beams[6]. However most such metasurfaces are passive in nature, and their response is fixed once they are fabricated.

Recently, there has been considerable interest in studying dynamically tunable metasurfaces, and many different mechanisms have been exploited to realize active metasurfaces[7]. These include voltage-induced re-orientation of molecules in a liquid crystal[8], the modulation of Fermi level in graphene via gating[9], phase change of a material upon heating or cooling[10], as well as field effect modulation of Fermi level in gallium arsenide[11], silicon[12] and transparent conducting oxides[13]. Notably, none of these mechanisms has yielded tunable metasurfaces operating in the visible wavelength range. This is partly due to challenges associated with obtaining large modulation of the complex refractive index of the constituent materials at visible wavelengths. For example, each element of a field effect tunable metasurface is effectively a metal-insulator-semiconductor capacitor, with the metal serving as a gate and the semiconductor functioning as a field effect channel [11-14]. When an electrical bias is applied between the metal gate and the semiconductor, charge depletion or accumulation layer is formed in the semiconductor at the semiconductor-insulator interface. The

This article is protected by copyright. All rights reserved.

Author Manuscript

complex dielectric permittivity of a semiconductor increases linearly with its carrier concentration, resulting in field effect optical modulation. On the other hand, dielectric permittivity of a semiconductor is inversely proportional to the light frequency squared, implying larger optical modulation will be observed at smaller frequencies (longer wavelengths). So far, field effect tunable metasurfaces have only been reported for wavelengths longer than 1.5 μm. The operating wavelength of graphene-based tunable metasurfaces has so far been limited to mid-infrared range[15]. This stems from the dielectric permittivity of graphene that is proportional to the square root of the carrier density in graphene and is inversely proportional to the square of the light frequency. Active tuning of the optical response of metasurfaces loaded with liquid crystal molecules has been previously demonstrated in the near-infrared wavelength range[8, 16]. However, anchoring of liquid crystal molecules to the surfaces of these structures is a major drawback of this approach. This issue has prevented the demonstration of tunable metasurfaces in the visible. Phase change materials have been previously used to demonstrate tunable metasurfaces in the mid- and near-infrared wavelength range[10, 17]. Although phase change materials exhibit refractive index modulation in the visible wavelength range, it is relatively modest relative to that in the near-infrared range. Here, we demonstrate tunable metasurfaces at visible wavelengths via a modulation mechanism based on ionic conductance, and also at strikingly low (single-millivolt scale) voltages.

Ionic conductance has been widely explored as a mechanism for electrochemical metallization-based resistive switching devices such as random access memories (RRAM)[18]. A prototypical RRAM device consists of two electrodes and an ionic conductor sandwiched between them. The ionic conductor, which can be an oxide[19-21], chalcogenide[22], or halide[23] material, permits ionic transport while preventing electron transport. In the case of simple cation movement-based RRAMs, one electrode is oxidizable (soluble), such as silver[19, 20] or copper[21], while the counter electrode is inert (insoluble). When a positive voltage is applied to the oxidizable electrode, its constituent metal starts to dissolve and starts depositing as a metallic filament at the opposite inert electrode (see **Figure** 1a). Upon increasing applied bias, the metallic filament ultimately bridges the relatively insulating ion conductor causing a large change in device resistance. Upon reversing the

This article is protected by copyright. All rights reserved.

Author Manuscript

bias, the filament starts to dissolve via ionic transport in the opposite direction, and the system microstructure evolves back towards its original state. Since ionic transport causes a significant change in the resistance of the medium, the modulation mechanism is usually referred to as resistive switching. Coupled electron-ion dynamics in resistive switching is able to realize the functional characteristic of a 'memristor' (memory-resistor) which was first theoretically proposed in 1971[24]. For this reason resistive switching in RRAM devices is also referred to as memristive switching[25].

Even though resistive switching was discovered almost fifty years ago[26], ionic conductance-based optical modulation in nanophotonic systems have been demonstrated only recently[27, 28]. Silver filament formation in thin amorphous silicon layer[27] or gold filament formation in thin silica layer[28] has been used to modulate transmittance of light through plasmonic waveguides upon application of a bias voltage. Active tuning of optical response of a plasmonic antenna attached to $Ag/Al_2O_3/Au$ memristive junction has also been experimentally demonstrated[29]. Active optical response of the antenna was attributed via indirect evidence to silver filament formation in a thin Al_2O_3 layer. A nanoparticle-on-mirror memristive switch for modulation of scattering was experimentally demonstrated which yielded few-percent changes in scattered intensity with ~1V applied bias[30], and it was argued that scattered intensity from the plasmonic cavity could be used as a probe of filament formation dynamics. A recent theoretical report[31] has suggested that electrochemical programming of the optical response of two adjacent Cu and Pt antennas via Cu filament formation in Cu_2S layer separating the antennas. Finally, it has been experimentally demonstrated that external bias-initiated local changes in ZnO stoichiometry in Al/ZnO/Si memristive antennas result in observable modulation of the reflected light at mid-infrared wavelengths[32]. Our tunable metasurface instead exploits a different mechanism that operates at very low (single-millivolt scale) voltages, an ionic transport-limited nucleation process in which Ag ion migration through a thin Al_2O_3 dielectric induces Ag nanoparticle nucleation and growth in the indium tin oxide (ITO) counter-electrode. This mechanism yields a large modulation of optical transmittance and reflectance at applied electric fields of 1 mV/nm, which is at least an order of magnitude lower than electric fields applied in the memristive optical modulation devices cited above. We would like to emphasize that in our device

This article is protected by copyright. All rights reserved.

Author Manuscript

observed millivolt-scale optical modulation is not accompanied by large changes in the device resistance as it is the case in previously reported ionic conduction-based optical modulators.

We first investigated the reflectance modulation of $Ag/Al_2O_3/ITO$ planar heterostructures when Ag is positively biased with respect to ITO, and then incorporated $Ag/Al_2O_3/ITO$ heterostructures into a metasurface to enhance the reflectance and transmittance modulation due to optical resonances supported by the structure.

The fabricated $Ag/Al_2O_3/ITO$ planar heterostructures consist of 80 nm thick Ag, 5 nm thick Al_2O_3 deposited via atomic layer deposition (ALD), followed by 110 nm of ITO sputtered onto the Al_2O_3 layer. The carrier concentration of the fabricated n-type ITO film is $5\times10^{20}/cm^3$. Transmission electron microscopy image of the fabricated sample is shown in Figure 1b. Before being measured, the sample has been left exposed to ambient environment for one week (*aged* sample). Reflectance measurements for *aged* planar structures under applied bias are shown in Figure 1c. The measurements are performed under normal incidence with applied bias ranging from 0 to 5 mV (with 1 mV steps). Upon application of a voltage, the reflectance decreases at longer wavelengths and increases at shorter wavelengths, with a crossover region at around 650 nm. The measured reflectance is much lower than that obtained from the simulations performed with complex refractive indices for constituent layers obtained via spectroscopic ellipsometry measurements performed for each constituent layer separately (see Supporting Information Part 2). We hypothesize that this could be due to migration of silver ions into alumina and possibly also into ITO. We assume that the effective refractive indices of composite media consisting of intermixtures of alumina and silver and intermixtures of ITO and silver can be

Author Manuscript

This article is protected by copyright. All rights reserved.

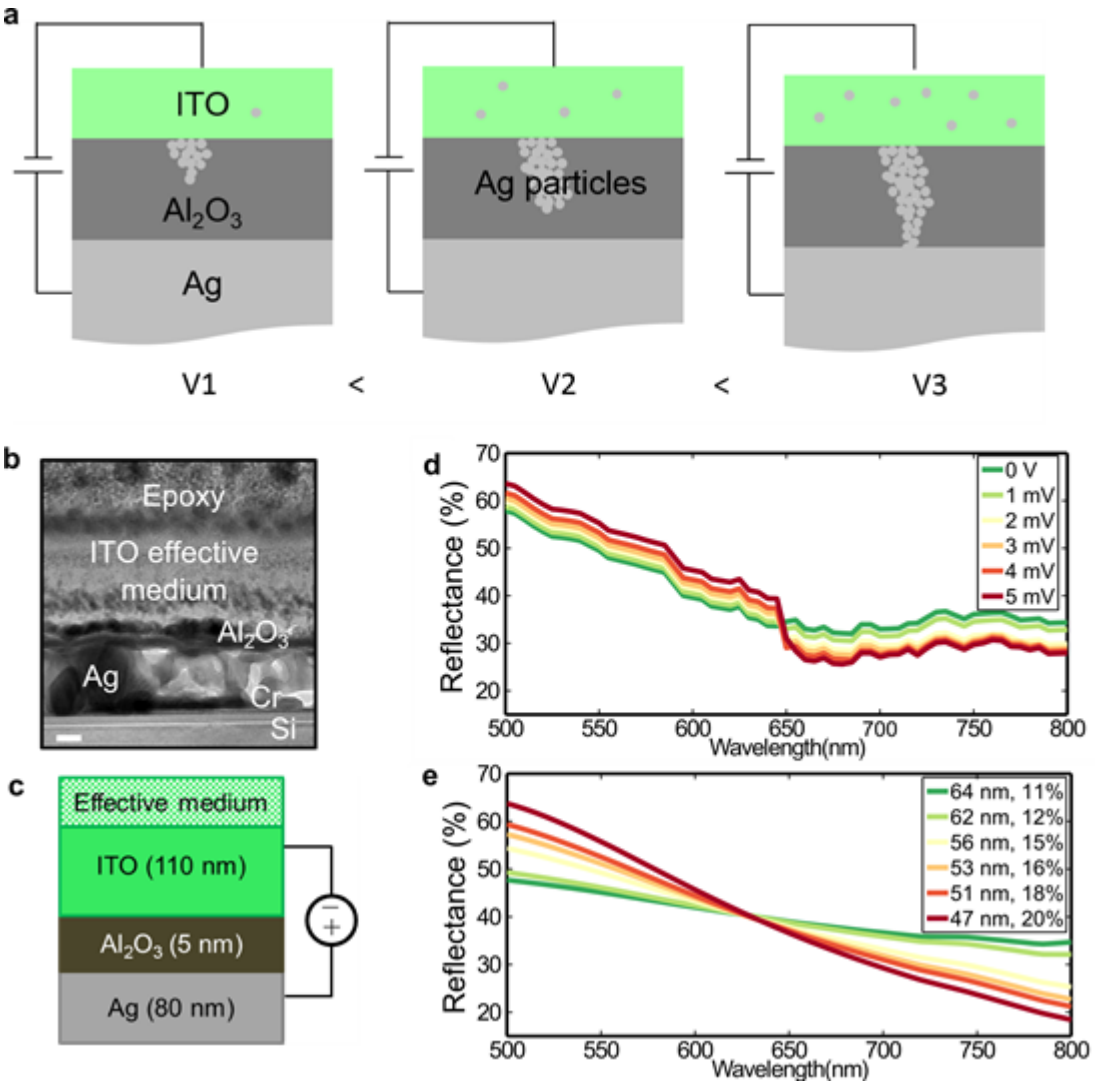

Figure 1. (a) Schematic showing the migration of silver ions and formation of silver filaments upon the application of an electrical bias; grey circles in Al_2O_3 and ITO represent silver nanoparticles, (b) Transmission Electron Microscopy images of the planar structures showing an effective medium formed in the layers, (c) schematic of the effective structure used for the simulations, (d) measured reflectance spectrum from $Ag/Al_2O_3/ITO$ planar heterostructure under applied bias voltages from 0 to 5 mV and (e) simulated reflectance from the planar heterostructure. The legend indicates the thickness of the effective medium layer along with corresponding fill fraction.

described by using an effective medium model in the Bruggeman approximation[33]. As a first step, we assume that Ag ions penetrate only into the 5 nm thick Al_2O_3 layer and calculate the reflectance from

This article is protected by copyright. All rights reserved.

$Ag/Al_2O_3/ITO$ planar stack. However the experimentally observed reflectance changes cannot be reproduced in simulations that assume Ag penetrates only into the thin Al_2O_3 layer. However simulations that also assume silver ion penetration into the 110 nm thick ITO layer are able to match the experimentally observed reflectance changes. Based on electron microscopy observations (see below), we modeled the ITO layer as being subdivided into two layers: i) a homogeneous layer of ITO located at the top interface of Al_2O_3 ii) a Ag nanoparticle-containing ITO layer which is treated as an effective medium, located between the homogeneous ITO layer and the free surface (see schematic shown in Figure 1c). Using the transfer matrix method, we calculate the reflectance from the multilayer stack and fit it to the experimentally measured curves. The thickness of the effective medium Ag/ITO layer and fill fraction of Ag in this layer are used as fitting parameters. The resulting simulations match the experimental data well (see Figure 1e). Each curve shown in Figure 1e corresponds to a distinct Ag nanoparticle fill fraction in the ITO layer and distinct thickness of the effective medium layer. Comparison of the fitted theoretical and experimental curves indicates that, when an electrical bias is applied, the effective medium layer shrinks in thickness from 64 nm to 47 nm, while the fill fraction of Ag nanoparticles in the effective medium layer increases from 11 % to 20 %. The legend in Figure 1e indicates the thickness of the effective medium layer along with the Ag nanoparticle fill fraction. Transmission electron microscopy images of the planar heterostructure indicate intermixing of Ag and ITO (Figure 1b).

Finally, to verify our hypothesis that the observed optical modulation is caused by migration of Ag ions, we obtained electron microscopy images of aged planar structures fabricated on Si substrates. In these samples, an additional 10 nm thick Al_2O_3 layer has been deposited on Si to electrically isolate the Ag layer and the underlying substrate. We performed electron microscopy imaging on two different aged planar structures: i) first sample has never been electrically modulated, ii) second sample was subjected to over one hundred modulation cycles with applied electrical biases ranging from 0 to 5 mV. The electron microscopy images gathered from an unmodulated sample are shown in **Figure** 2a and 2b. One can clearly see well-defined material layers with no material intermixing. On the other hand, the images taken from the repeatedly modulated sample are given in

This article is protected by copyright. All rights reserved.

Author Manuscript

Figure 2c-2g. Figure 2c shows that there are 5-12 nm diameter particles in ITO, which increase in concentration and size near the ITO/air interface (see encircled region). Local energy-dispersive X-ray spectroscopy (EDS) measurements indicate a Ag fraction of up to 5.2% in those regions of the ITO. Figure 2d and 2f show electron microscopy images for samples that have been repeatedly modulated with bias voltages from 0 to 5 mV. The high magnification images in Figure 2d-2g reveal a polycrystalline material which appears to be Ag intermixed with Al_2O_3. Figure 2d (2f) is identical to Figure 2e (2g) but the spatial regions of intermixture of the Al_2O_3 and Ag are highlighted with dashed outlines. These images confirm that the observed optical modulation is indeed due to migration of Ag ions under applied bias (for additional TEM images and EDS data see Supporting Information Part 3-6). Previously, conducting Ag filament formation in $Ag/Al_2O_3/ITO$ memristive structures has been imaged via dual beam time-of-flight secondary ions mass spectrometry[34]. It has been observed that under applied bias Ag ions may penetrate into ITO for hundreds of nanometers, which is consistent with our results. In our case, no electroforming step is necessary to trigger the ion migration process. Other work analyzing the resistive switching in $Pt/TiO_2/Pt$ structures also indicated that no electroforming process is necessary to trigger ionic transport when the gate dielectric is thinner than 6 nm[35]. On the other hand, resistive switching under millivolt bias with no prior electroforming step has been recently observed in a $Pt/TiO_2/TiN$ structure[36]. The thickness of TiO_2 in this structure was 70 nm. This observation suggests that the presence of the TiN top electrode is crucial for elimination of electroforming and ultralow bias operation. Similarly, our results suggest that the ITO electrode is essential for observation of optical

Author Manuscript

This article is protected by copyright. All rights reserved.

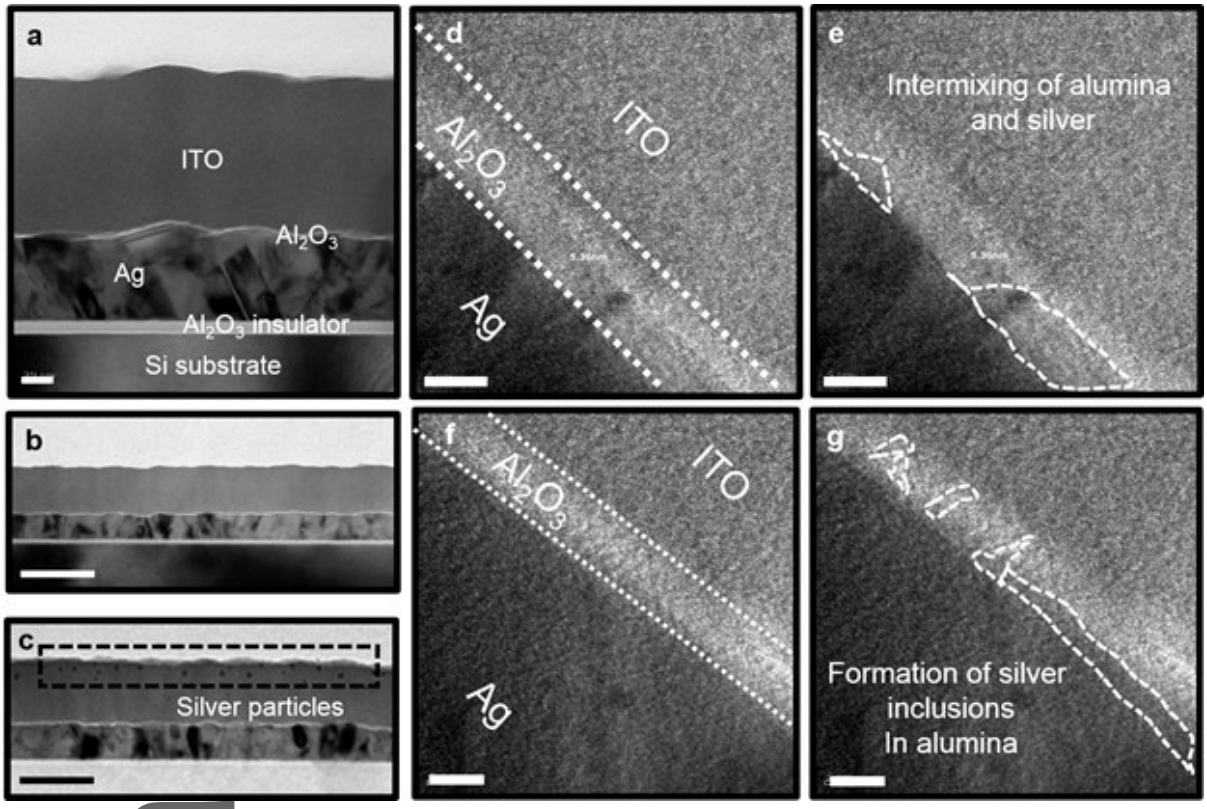

Figure 2. TEM images of the cross-section of the planar structure. (a) a sample that has never been electrically modulated; (b) a compressed image of (a); (c) a sample that has been subject to > 103 cycles of electrical bias modulation thereby showing the presence of silver up even inside the ITO layer (dark spots encircled in a back dashed rectangle); scale bars in (b) and (c) correspond to 80 nm; the compressed image (b) is depicted for facilitating the comparison with (c); (d)-(g) magnified image of the interface between Ag/Al_2O_3/ITO of the heavily electrically modulated sample shown in (c). The scale bar in (d)-(g) is 5 nm. (d) shows intermixing of Al_2O_3 and silver in the dielectric layer and (f) shows formation of silver inclusions inside the Al_2O_3 layer. Parts (e) and (g) are identical to (d) and (f), except that the regions of interest have been highlighted by white dashed lines.

modulation under millivolt bias. By contrast, an applied bias voltage on the order of volts was required to enable optical modulation in Ag/Al_2O_3/Au crossbar antenna devices[29] – which do not contain ITO – even though the Al_2O_3 layer was only 5 nm thick. For Pt/TiO_2/Pt structures, it is known that resistive switching occurs due to movement of oxygen vacancies. In case of the Ag/Al_2O_3/ITO heterostructures studied here, both migration Ag ions and oxygen vacancies are likely contributors to

This article is protected by copyright. All rights reserved.

Author Ma

transport and device operation. Indeed, it has been previously demonstrated that ITO layers incorporated in a memristive device can absorb or provide oxygen vacancies under an applied bias[37]. Furthermore, one may imagine that the change in ionic concentration at the ITO and ITO/Al_2O_3 interface may be dictating the observed optical modulation. However this conjecture can be disproved by looking at the TEM images as shown in Figure 2b and 2c. It can be seen that the silver nanoparticles actually penetrate into the ITO and that there are no particles located at the ITO and ITO/Al_2O_3 interface. In addition to this, simulations on the planar interfaces show indeed that the observed modulation can be explained by incorporating silver nanoparticles into an effective medium like approximation, as seen in Figure 1d and 1e. This thus leads us to believe that the observed phenomenon is in fact of a new origin.

Next, we incorporate Ag/Al_2O_3/ITO tunable heterostructures into a metasurface. Optical resonances supported by the metasurface enhance light-matter interactions, resulting in larger tunability of the reflectance and transmittance when a bias voltage is applied. The fabricated tunable metasurface consists of quartz substrate, 1 nm Cr adhesion layer, followed by 80 nm thick Ag in which inverse dolmen structures have been milled using focused ion beam lithography (see **Figure** 3a-3c). The inverse dolmen structure consists of two lower parallel rods and a top rod. The lower parallel rods are 150 nm long and 100 nm wide, and their mutual spacing is 30 nm. Both of these are 30 nm away from a 230 nm long and 100 nm wide top rod. A scanning electron microscope image of an array of fabricated inverse dolmen structures is shown in Figure 3c. Next, we conformally deposit 5 nm Al_2O_3 films via atomic layer deposition, and 110 nm of ITO via RF magnetron sputtering. A schematic of the light-matter interaction in such structures is shown in Figure 3a, with the inset depicting different layers. The total area of the fabricated inverse dolmen structures is 200 μm × 200 μm. Figure 3b shows a schematic of the cross-section of the structure.

Author Manuscript

This article is protected by copyright. All rights reserved.

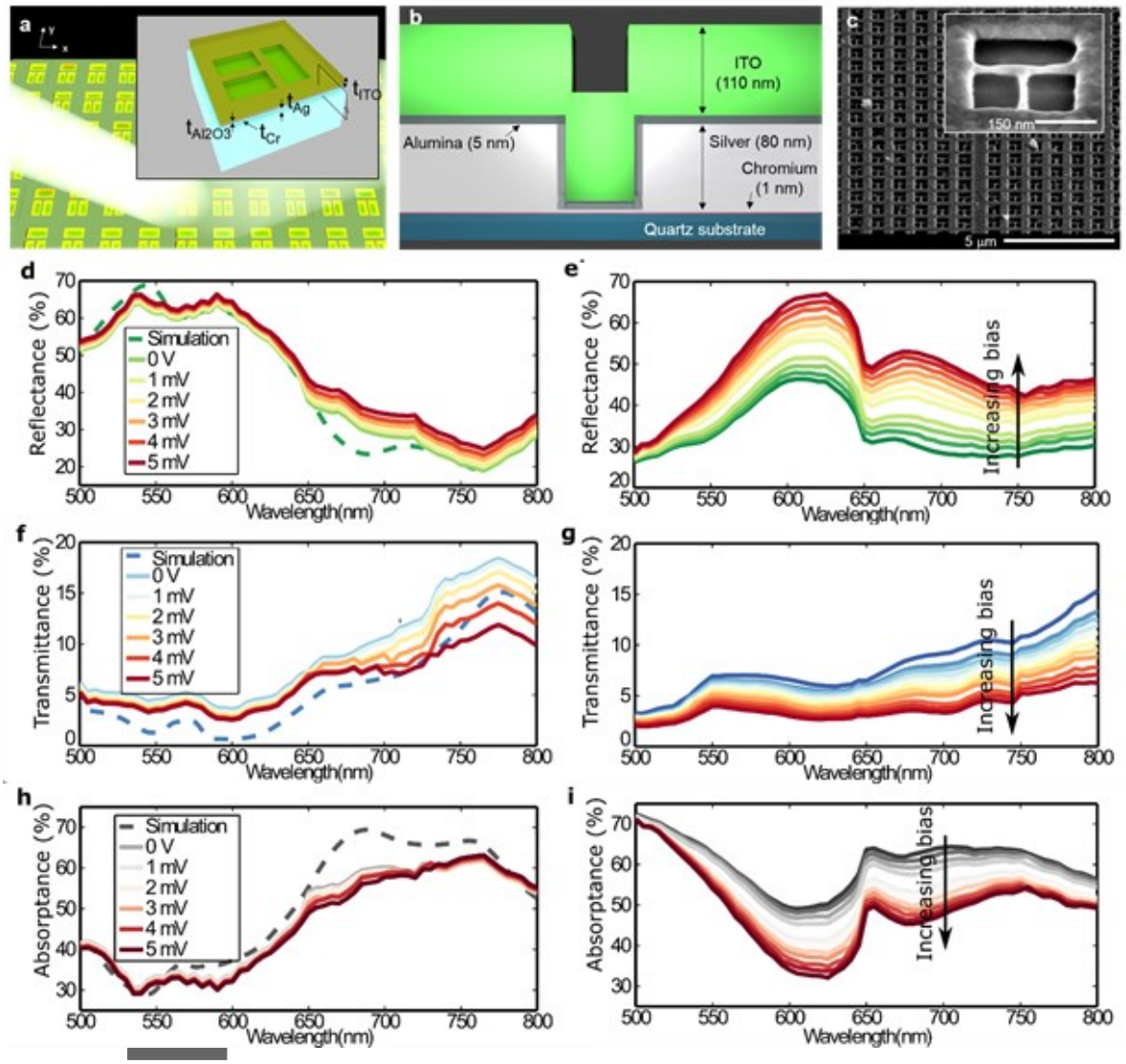

Figure 3. (a) Schematic of the envisioned light-matter interaction in the metasurface with dimensions mentioned, (b) cross-section showing the different layers in the structures, (c) SEM images of the inverse dolmen structures showing an array and individual configuration, optical measurements of (d), (e) reflectance, (f), (g) transmittance and (h), (i) absorptance spectra at normal incidence for fresh and aged dolmen samples respectively. The dashed lines show simulation results at no applied bias, while the solid lines represent the experimental results under applied bias from 0 mV to 5 mV. Applied bias varies from 0 to 5 mV with incremental steps of 0.5 mV.

When milling inverse dolmen structures into a silver film, a thin silver layer was left at the bottom of the device (between chromium and bottom Al_2O_3 layers). Two sets of inverse dolmen

This article is protected by copyright. All rights reserved.

Author

samples were measured, (i) first set of samples was measured immediately upon fabrication (fresh samples) (ii) second set of samples had been left exposed to ambient environment for a week before being measured (aged samples). Interestingly, we observe that reflectance and transmittance spectra of the fresh samples differ from the spectra obtained from the aged samples. Moreover, aged samples show much greater optical reflectance and transmittance modulation than the fresh ones. We believe that the origin of the 'aged sample effect' can be attributed to the contamination of the samples by chlorine and sulphur, both of which are known to assist in the mobility of silver ions and ease in formation of ions[38]. The results of the optical measurements performed on fresh samples are shown in Figure 3d, 3f and 3h. First, measurements were taken at zero bias and subsequently silver electrode was positively biased with respect to ITO electrode. Upon the application of a 5 mV bias (in 5 steps, leading to each incremental graph representing a bias of 1 mV), the reflectance of fresh samples exhibits a broadband relative increase by up to 9% that corresponds to the absolute reflectance increase by nearly 6%. The relative reflectance increase is defined by 100× [R(5mV)-R(0mV)]/ R(0mV), where R(0mV) and R(5mV) stand for reflectance values at no applied bias and 5 mV of bias, respectively. As one can see from Figure 3f, the measured transmittance exhibits a broadband relative decrease by up to 35% that corresponds to the absolute transmittance decrease by around 6%. Interestingly, upon bias voltage application, dips and peaks observed in reflectance and transmittance do not change their spectral position. Results of the full wave electromagnetic simulations under no applied bias are indicated by dashed lines (for further details see Supporting Information Part 7). As one can see, in the case of fresh samples, the simulated and experimental curves match reasonably well. Next, we performed optical measurements on aged dolmen samples. Reflectance and transmittance spectra measured under an applied bias are shown in Figure 2e, g, and i. As one can see, the aged samples show a much larger reflectance modulation than fresh ones: we observe relative reflectance increase by 30% (15% absolute increase) and relative transmittance decrease by 33% (5% absolute decrease) upon application of a 5 mV bias voltage. Spectral characteristics of the aged samples at zero bias are also different from those obtained from fresh samples: aged samples show lower reflectance at shorter wavelengths and higher transmittance at longer wavelengths. For

This article is protected by copyright. All rights reserved.

Author Manuscript

increasing bias voltages, the reflectance increases until it reaches an absolute maximum saturation value of 90% upon the application of 6 mV (see Supporting Information Part 8). Thereafter, there is a steep reduction in the reflectance, tailing down at 12% beyond which there is a dramatic increase in the leakage current. This gives a strikingly large dynamic range of absolute reflectance change by ΔR = 78% with the application of just 100 mV (for additional optical measurements, see Supporting Information Parts 9-11). We have also performed cyclic voltammetry measurements on aged dolmen samples. We observe a pinched hysteresis loop in a plot of current versus voltage that is a signature of a memristive system[39] (see Supporting Information Part 13). One of the important figures of merit of RRAM devices is defined by the ratio of the device resistances in the on and off states[18]. However, within the context of ionic conductance-based optical modulators the change of the device resistance is not an important metric any more since large optical modulation can still be observed without considerable resistance changes. For example, under millivolt electrical bias our device shows significant optical modulation without large changes in resistance.

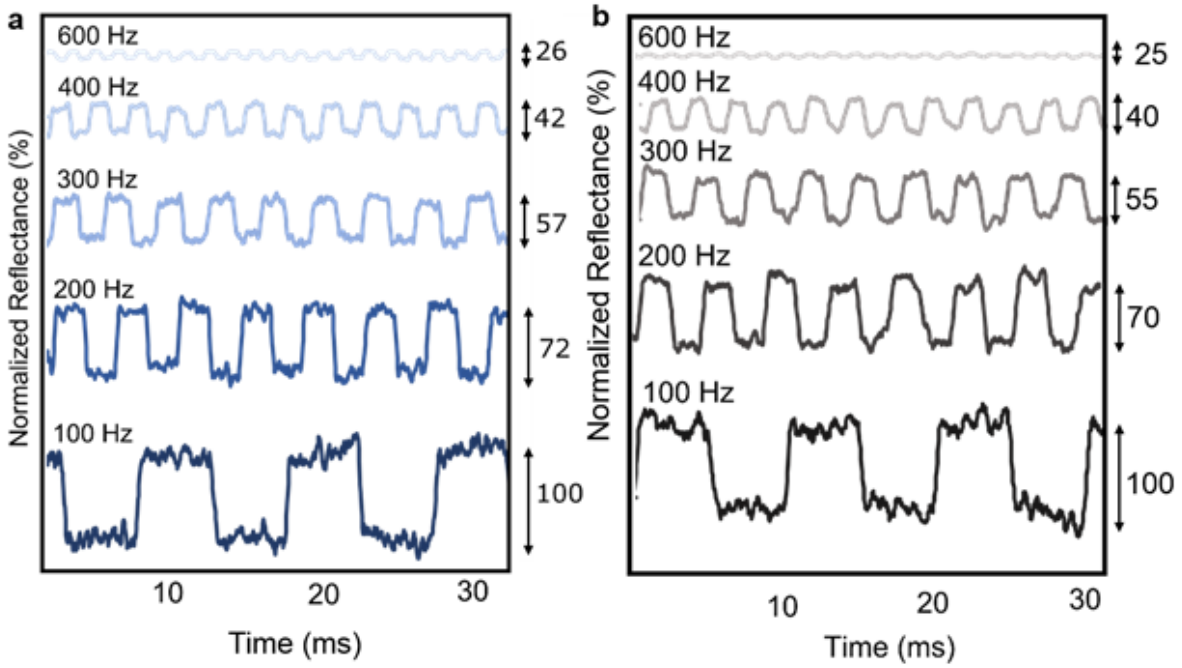

Figure 4. Reflectance signal as a function of time for different modulation frequencies for (a) an aged dolmen metasurface and (b) an aged planar structure. In cases of both planar structures and metasurfaces reflectance values are normalized to the values of the reflectance change obtained at 100 Hz modulation frequency.

This article is protected by copyright. All rights reserved.

Manuscript Accepted

Hence, in this regime, the distribution of silver ions in our device can be schematically described by the middle panel of Figure 1a.

Finally, we identify the response time of the fabricated devices. To characterize the frequency response of the aged planar structures as well as aged dolmen metasurfaces, a 5 mV bias, with frequencies ranging from 100 to 600 Hz, was applied and a high speed Si detector was used to detect the reflectance from the structures. The measurements have been done at the wavelength of λ=700 nm. The reflectance values plotted in **Figure** 4a-4b are normalized to the values of reflectance change obtained at 100 Hz modulation frequency. As modulation frequency increases, the amplitude of the modulated signal decreases. At modulation frequency of 600 Hz, the recorded normalized signal is almost flat implying that the silver ions are unable to get fully rearranged upon electrical modulation. Thus, frequency response of planar structures and inverse dolmen metasurfaces is very similar. We can make an estimate of the silver nanoparticle formation dynamics by looking at the transmission electron microscopy images shown in Figure 2b and 2c and referring to Figure 4. From Figure 2b we note the radius of the bigger silver nanoparticles is 10-12 nm. For a density of FCC silver of 10.5 g/cm^3, the mass of a single silver nanoparticle is of order of $4.4x10^{-20}$ kg. Considering the total sample area and the thickness of ITO, the volume into which silver ions can penetrate is roughly $1.38x10^{-14}$ m^3. From Figure 1d and 1e, we can estimate the volume of silver penetrated into ITO at the two extreme biases of 0V and 5 mV, yielding fill fractions of 11% and 20%, and Ag volumes of $1.52x10^{-15}$ m^3 and $2.76x10^{-15}$ m^3 respectively. In turn, we obtain a number of silver atoms moving into or out of the ITO of $3.63x10^8$ and $6.6x10^8$ respectively, at the two fill fractions. Since silver ions have unit charge, we can estimate the amount of charge passed into or out of the ITO volume at 0V and 5 mV biases. For the 100 Hz signal modulation at 5 mV in Figure 4, we obtain a charge movement of $2.75x10^{-11}$ C in 1 ms. This corresponds to a current of 27.5 nA, which compares to a value of 15 nA obtained in our IV plots in the Supporting Information (see Figure S16). This quick calculation supports our hypothesis that the AC modulation current is sufficient to explain the Ag ion transport needed to nucleate the nanoparticles that give rise to optical modulation. The moderate modulation

This article is protected by copyright. All rights reserved.

Author Manuscript

frequency reported here is partially due to large device area (1 mm × 1 mm) that results in large RC constant. When studying Ag ion migration in small-area Ag/ZnO:Mn/Pt device, switching frequencies on the order of 100 MHz have been observed[19]. Since power consumption of an electronic device scales as $P = CV^2f$, where C is the capacitance of the device, V is the applied bias, and f is the modulation frequency, shrinking area of our device could pave a route towards ultralow-power optical modulators.

In this Communication, we have experimentally demonstrated an ultralow voltage optical modulator exhibiting absolute reflectance modulation by up to 78% with a bias of 100 mV (and absolute reflectance increase by 15% with a bias of just 5 mV). Our system exploits a new mechanism of ionic conductance-mediated nucleation and growth of Ag nanoparticles to modulate the optical reflectance and transmittance. Since complex dielectric permittivity values of ITO and Ag are very different in a broad wavelength range, one may expect that the reported modulation mechanism may yield active optical devices for wavelengths extending beyond visible (see Supporting Information Part 14). The results represent an advance over previous work[27, 28-30] by revealing a new mechanism that operates at dramatically lower electric fields, yielding a reduction of the applied bias voltages for optical reflectance modulation by three orders of magnitude.

Our work could be used for design of future attojoule-energy scale optical modulators, highly sensitive optical readout of surface phenomena, optical display technology, and non-volatile optical memories.

Experimental Section

Fabrication and Characterization of Planar Ag/Al_2O_3/ITO *Heterostructures:* To fabricate Ag/Al_2O_3/ITO planar heterostructures, we evaporate a 1 nm Cr adhesion layer and 80 nm of Ag, using electron beam deposition, on either Si or SiO_2 substrates. Next, we deposit 5 nm of Al_2O_3 via atomic layer deposition (ALD) and 110 nm of ITO via RF magnetron sputtering (O_2 flow rate of 0.5 sccm). The samples fabricated on SiO_2 substrate were used to perform optical measurements. The samples fabricated on Si substrates contain a 10 nm thick Al_2O_3 buffer layer that electrically insulates

This article is protected by copyright. All rights reserved.

Author Manuscript

$Ag/Al_2O_3/ITO$ planar stack from Si (Figure 1b). The samples on Si substrate are used for transmission electron microscopy (TEM) imaging. Materials characterization of the ITO revealed the carrier concentration and permittivity, using Van der Pauw Hall measurements and spectroscopic ellipsometry, respectively. The resulting film was n-type with a carrier concentration of $5\times10^{20}/cm^3$. To perform Hall measurements, we deposited 110 nm of ITO on SiO_2 substrates, while for ellipsometry measurements, 110 nm of ITO was deposited on Si substrates. The 5 nm layer of ALD-deposited Al_2O_3 was repeatedly tested for the leakage current and it was seen that most of the samples were displaying very good insulation properties. For a device with area of 1 mm × 1 mm a 5-10 nA leakage current has been observed. The planar samples on SiO_2 substrate enable one to perform both reflectance and transmittance measurements. However, due to the large Ag thickness, the measured transmittance was negligibly small.

Optical measurements: Optical measurements under applied bias were undertaken at normal incidence. A microscope objective 5 X (Olympus, NA 0.6) was used to focus incident light from a supercontinuum laser light source to a spot of size roughly 20 microns, and the signal was measured using a Si detector. Measurements were taken for a wavelength range from 500 nm to 800 nm. For the bias dependent measurements, a voltage was applied using a voltage source. The bias was applied between the top layer of ITO and the bottom layer of silver at locations far from the measured area.

a) *Transmission Electron Microscopy*: Transmission electron microscopy/ energy-dispersive X-ray spectroscopy (EDS) analysis was performed with FEI TF30ST transmission electron microscope at an accelerating voltage of 300 kV.

Fabrication of the Tunable Metasurface: To fabricate the tunable metasurface, we evaporate a 1 nm chromium adhesion layer and 80 nm of silver, using electron beam deposition, on a quartz substrate. Focused ion beam lithography is carried out on the deposited silver film to create a metasurface of inverse dolmen structures (see Figure 3a-3c). Next, we deposit 5 nm Al_2O_3 films via atomic layer deposition, and 110 nm of ITO via RF magnetron sputtering (O_2 flow rate of 0.5 sccm). When milling inverse dolmen structures into a silver film, a thin silver layer was left at the bottom of

This article is protected by copyright. All rights reserved.

Author Manuscript

the device (between chromium and bottom Al_2O_3 layers). All the deposition steps are undertaken with appropriate face masks made of stainless steel, to permit an easy bias application configuration in the final device. A transmission electron microscopy image of an identical planar heterostructure ($Cr/Ag/Al_2O_3/ITO$) deposited on a silicon substrate showed a uniform layer of roughly 1.2 nm of chromium as the adhesion layer (see Figure S3 of Supporting Information) and hence no disconnected islands of chromium were created.

Scanning Electron Microscopy (SEM) and EDS: Dualbeam Focused Ion Beam with X-Ray microanalysis FEI Nova 200 Nanolab was used to gather SEM images. The same tool was used to perform EDS characterization of the dolmen samples (see Supporting Information Part 5 and 6). Besides detecting the presence of silver, oxygen, indium, and tin, a finite sulphur and chlorine signal was present throughout, wherever silver was present, for the aged sample. The presence of sulphur and chlorine are attributed to silver tarnishing upon air exposure during the fabrication process and during subsequent ambient atmosphere exposure.

Calculation of the Optical Response of the Structures: The reflectance from $Ag/Al_2O_3/ITO$ planar heterostructures was calculated by using transfer matrix method. Effective dielectric permittivity of the composite media consisting of intermixtures of Al_2O_3 and Ag and intermixtures of ITO and Ag is described by using an effective medium model in the Bruggeman approximation. We perform full-wave simulations to calculate the optical response of the designed inverse dolmen metasurface (Supporting Information Part 7). For our full-wave simulations we use finite-difference time-domain method.

Supporting Information

Supporting Information is available from the Wiley Online Library or from the author.

Acknowledgements

This work was supported by the Swiss National Science Foundation (Grant number 151853), Hybrid Nanophotonics Multidisciplinary University Research Initiative Grant (Air Force Office of Scientific

This article is protected by copyright. All rights reserved.

Author Manuscript

Research, FA9550-12-1-0024) and the Samsung Electronics Metaphotonics Cluster. The conducting oxide material synthesis design and characterization was supported by the U.S. Department of Energy (DOE), Office of Science Grant (DE-FG02-07ER46405). Used facilities were supported by the Kavli Nanoscience Institute (KNI) and Joint Center for Artificial Photosynthesis (JCAP) at Caltech. The authors would like to thank Artur R. Davoyan, Matthew Sullivan Hunt and Barry Baker for useful discussions, Carol Garland for help with the TEM imaging, and Jonathan Grandidier for his help with the transfer matrix code.

Author Manuscript

References

[1] J. Wang, J. Du, *Appl. Sci--Basel* **2016**, *6*, 239.

[2] A. Arbabi, Y. Horie, M. Bagheri, A. Faraon, *Nat. Nanotech.* **2015**, *10*, 937.

[3] D. Veksler, E. Maguid, N. Shitrit, D. Ozeri, V. Kleiner, E. Hasman, *Acs Photonics* **2015**, *2*, 661; A. Pors, M. G. Nielsen, R. L. Eriksen, S. I. Bozhevolnyi, *Nano Lett.* **2013**, *13*, 829; N. F. Yu, F. Capasso, *Nat. Mater.* **2014**, *13*, 139.

[4] W. T. Chen, K.-Y. Yang, C.-M. Wang, Y.-W. Huang, G. Sun, I.-D. Chiang, C. Y. Liao, W.-L. Hsu, H. T. Lin, S. Sun, L. Zhou, A. Q. Liu, D. P. Tsai, *Nano Lett.* **2014**, *14*, 225; G. Zheng, H. Muhlenbernd, M. Kenney, G. Li, T. Zentgraf, S. Zhang, *Nat. Nanotech.* **2015**, *10*, 308; Y.-W. Huang, W. T. Chen, W.-Y. Tsai, P. C. Wu, C.-M. Wang, G. Sun, D. P. Tsai, *Nano Lett.* **2015**, *15*, 3122; X. J. Ni, A. V. Kildishev, V. M. Shalaev, *Nat. Commun.* **2013**, *4*, 2807.

[5] C. Pfeiffer, C. Zhang, V. Ray, L. J. Guo, A. Grbic, *Optica* **2016**, *3*, 427.

[6] J. Du, J. Wang, *Sci. Rep.* **2015**, *5*, 9662.

[7] M. Ferrera, N. Kinsey, A. Shaltout, C. DeVault, V. Shalaev, A. Boltasseva, *J. Opt. Soc. Am. B* **2017**, *34*, 95.

[8] O. Buchnev, N. Podoliak, M. Kaczmarek, N. I. Zheludev, V. A. Fedotov, *Adv. Opt. Mater.* **2015**, *3*, 674.

[9] V. W. Brar, M. S. Jang, M. Sherrott, J. J. Lopez, H. A. Atwater, *Nano Lett.* **2013**, *13*, 2541.

[10] M. J. Dicken, K. Aydin, I. M. Pryce, L. A. Sweatlock, E. M. Boyd, S. Walavalkar, J. Ma, H. A. Atwater, *Opt. Express* **2009**, *17*, 18330.

[11] Y. C. Jun, J. Reno, T. Ribaudo, E. Shaner, J. J. Greffet, S. Vassant, F. Marquier, M. Sinclair, I. Brener, *Nano Lett.* **2013**, *13*, 5391.

[12] A. Olivieri, C. Chen, S. Hassan, E. Lisicka-Skrzek, R. N. Tait, P. Berini, *Nano Lett.* **2015**, *15*, 2304.

[13] Y. W. Huang, H. W. H. Lee, R. Sokhoyan, R. A. Pala, K. Thyagarajan, S. Han, D. P. Tsai, H. A. Atwater, *Nano Lett.* **2016**, *16*, 5319.

[14] J. Park, J. H. Kang, X. G. Liu, M. L. Brongersma, *Sci. Rep.* **2015**, *5*, 15754.

[15] M. C. Sherrott., Philip W.C. Hon, Katherine T. Fountaine, Juan C. Garcia, Samuel M. Ponti, Victor W. Brar, Luke A. Sweatlock, H. A. Atwater, *DOI:10.1021/acs.nanolett.7b00359*; N. Dabidian, I. Kholmanov, A. B. Khanikaev, K. Tatar, S. Trendafilov, S. H. Mousavi, C. Magnuson, R. S. Ruoff, G.

This article is protected by copyright. All rights reserved.

Shvets, *Acs Photonics* **2015**, *2*, 216; Y. Yao, M. A. Kats, P. Genevet, N. F. Yu, Y. Song, J. Kong, F. Capasso, *Nano Lett.* **2013**, *13*, 1257.
[16] J. Sautter, I. Staude, M. Decker, E. Rusak, D. N. Neshev, I. Brener, Y. S. Kivshar, *Acs Nano* **2015**, *9*, 4308; M. Decker, C. Kremers, A. Minovich, I. Staude, A. E. Miroshnichenko, D. Chigrin, D. N. Neshev, C. Jagadish, Y. S. Kivshar, *Opt. Express* **2013**, *21*, 8879.
[17] Y. G. Chen, T. S. Kao, B. Ng, X. Li, X. G. Luo, B. Luk'yanchuk, S. A. Maier, M. H. Hong, *Opt. Express* **2013**, *21*, 13691; B. Gholipour, J. F. Zhang, K. F. MacDonald, D. W. Hewak, N. I. Zheludev, *Adv. Mater.* **2013**, *25*, 3050.
[18] F. Pan, S. Gao, C. Chen, C. Song, F. Zeng, *Mat. Sci. Eng. R.* **2014**, *83*, 1.
[19] Y. C. Yang, F. Pan, Q. Liu, M. Liu, F. Zeng, *Nano Lett.* **2009**, *9*, 1636.
[20] Y. C. Yang, P. Gao, S. Gaba, T. Chang, X. Q. Pan, W. Lu, *Nat. Commun.* **2012**, 3:732.
[21] S. Yazdanparast, J. A. Koza, J. A. Switzer, *Chem. Mater.* **2015**, *27*, 5974.
[22] F. Zhuge, K. Li, B. Fu, H. L. Zhang, J. Li, H. Chen, L. Y. Liang, J. H. Gao, H. T. Cao, Z. M. Liu, H. Luo, *Aip Adv.* **2015**, *5*, 057125
[23] X. F. Liang, Y. Chen, L. Shi, J. Lin, J. Yin, Z. G. Liu, *J. Phys. D Appl. Phys.* **2007**, *40*, 4767.
[24] L. O. Chua, *IEEE Transactions on Circuit Theory* **1971**, ct-18, 507.
[25] J. J. Yang, M. D. Pickett, X. M. Li, D. A. A. Ohlberg, D. R. Stewart, R. S. Williams, *Nat. Nanotech.* **2008**, *3*, 429.
[26] T. W. Hickmott, *J. Appl. Phys* **1962**, *33*, 2669.
[27] A. Emboras, I. Goykhman, B. Desiatov, N. Mazurski, L. Stern, J. Shappir, U. Levy, *Nano Lett.* **2013**, *13*, 6151; A. Emboras, J. Niegemann, P. Ma, C. Haffner, A. Pedersen, M. Luisier, C. Hafner, T. Schimmel, J. Leuthold, *Nano Lett.* **2016**, *16*, 709.
[28] C. Hoessbacher, Y. Fedoryshyn, A. Emboras, A. Melikyan, M. Kohl, D. Hillerkuss, C. Hafner, J. Leuthold, *Optica* **2014**, *1*, 198.
[29] D. T. Schoen, A. L. Holsteen, M. L. Brongersma, *Nat. Commun.* **2016**, 7:12162.
[30] G. Di Martino, S. Tappertzhofen, S. Hofmann, J. Baumberg, *Small* **2016**, *12*, 1334.
[31] S. Dong, K. Zhan, Z. P. Yu, J. A. Fan, *Acs Nano* **2016**, *10*, 6716.
[32] E. Battal, A. Ozcan, A. K. Okyay, *Adv. Opt. Mater.* **2014**, *2*, 1149.
[33] G. A. Niklasson, C. G. Granqvist, O. Hunderi, *Appl. Optics* **1981**, *20*, 26.
[34] Y. Busby, S. Nau, S. Sax, E. J. W. List-Kratochvil, J. Novak, R. Banerjee, F. Schreiber, J. J. Pireaux, *J. Appl. Phys.* **2015**, *118*, 075501.
[35] J. J. Yang, F. Miao, M. D. Pickett, D. A. A. Ohlberg, D. R. Stewart, C. N. Lau, R. S. Williams, *Nanotechnology* **2009**, *20*, 215201.
[36] A. Al-Haddad, C. L. Wang, H. Y. Qi, F. Grote, L. Y. Wen, J. Bernhard, R. Vellacheri, S. Tarish, G. Nabi, U. Kaiser, Y. Lei, *Acs Appl. Mater. Inter.* **2016**, *8*, 23348.
[37] E. O. Filatova, A. P. Baraban, A. S. Konashuk, M. A. Konyushenko, A. A. Selivanov, A. A. Sokolov, F. Schaefers, V. E. Drozd, *New J. Phys.* **2014**, *16*, 113014; T.-C. C. Chih-Hung Pan, Tsung-Ming Tsai, Kuan-Chang Chang, Tian-Jian Chu, Chih-Cheng Shih, Chih-Yang Lin, Po-Hsun Chen, Huaqiang Wu, Ning Deng, He Qian, and Simon M. Sze, *IEEE Transactions on Electron. Devices* **2016**, *63*, 4737.
[38] H. K. Hardy, *Prog. Met. Phys.* **1956**, 6, 45; G. W. Luckey, *Discuss. Faraday Soc.* **1959**, *28*, 113; S. P. Xie, X. C. Zhang, D. Xiao, M. C. Paau, J. Huang, M. M. F. Choi, *J. Phys. Chem. C* **2011**, *115*, 9943; Y. X. Zhang, S. D. Sun, X. Z. Zhang, L. L. Tang, X. P. Song, Z. M. Yang, *Phys. Chem. Chem. Phys.* **2014**, *16*, 18918.
[39] R. Tetzlaff, *Memristors and memristive systems*, Springer, New York 2014; Y. C. Yang, W. Lu, Nanoscale **2013**, *5*, 10076.

This article is protected by copyright. All rights reserved.

Author Manuscript

Author Manuscript

This article is protected by copyright. All rights reserved.

We demonstrate a new physical mechanism for electrical modulation of the optical response of a metasurface. The proposed mechanism is based on transport of silver ions into indium tin oxide (ITO) and subsequent nucleation and growth of silver nanoparticles inside ITO. This phenomenon yields 30% relative change in reflectance of a metasurface at strikingly low (single-millivolt scale) modulation voltages.

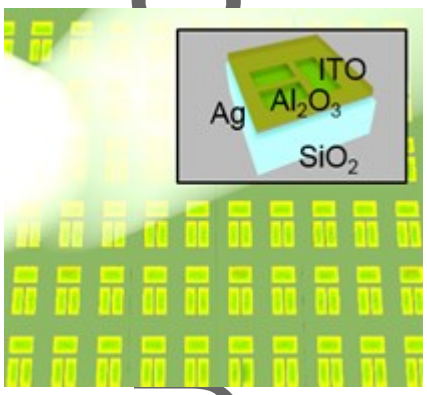

Author Manuscript

This article is protected by copyright. All rights reserved.